Dalton Transactions

PAPER

Check for updates

Cite this: *Dalton Trans.*, 2019, **48**, 14312

Hydrogen peroxide adducts of triarylphosphine oxides†

Fabian F. Arp, Nattamai Bhuvanesh and Janet Blümel *

Received 26th July 2019,
Accepted 27th August 2019

DOI: 10.1039/c9dt03070k

rsc.li/dalton

Five new hydrogen peroxide adducts of phosphine oxides $(p\text{-}Tol_3PO{\cdot}H_2O_2)_2$ (**1**), $(o\text{-}Tol_3PO{\cdot}H_2O_2)_2$ (**2**), $(o\text{-}Tol_2PhPO{\cdot}H_2O_2)_2$ (**3**), $(p\text{-}Tol_3PO)_2{\cdot}H_2O_2$ (**4**), and $(o\text{-}TolPh_2PO)_2{\cdot}H_2O_2$ (**5**), and the water adduct $(o\text{-}Tol_2PhPO{\cdot}H_2O)_2$ (**6**) have been synthesized and fully characterized. Their single crystal X-ray structures have been determined and analyzed. The IR and ^{31}P NMR data are in accordance with strong hydrogen bonding of the hydrogen peroxide. The mono- *versus* dimeric nature of the adduct assemblies has been investigated by DOSY NMR experiments. Raman spectroscopy of the symmetric adducts and the ν(O–O) stretching bands confirm the presence of hydrogen-bonded hydrogen peroxide in the solid materials. The solubilities in organic solvents have been quantified. Due to the high solubilities of **1–6** in organic solvents their ^{17}O NMR spectra could be recorded in natural abundance, providing well-resolved signals for the P=O and O–O groups. The adducts **1–5** have been probed regarding their stability in solution at 105 °C. The decomposition of the adduct **1** takes place by loss of the active oxygen atoms in two steps.

1. Introduction

Peroxides are ubiquitous in daily life.[1] They are active ingredients for disinfecting and bleaching in the production of goods,[2] the household, and wastewater treatment. Recently, H_2O_2 has been shown to break down polymers.[3] Artemisinin and related species play roles as antiparasitic and anti-malarial agents.[4] Peroxides are also employed in industry, for example, as radical initiators of polymerizations,[1b] and they play central roles in synthetic chemistry.[1] Recent applications include the oxidation of amines[5] and sulfides,[6] alkane activation,[7] and epoxidations.[8] Our group[9–18] and others[19–23] study all aspects of phosphine oxidation. Furthermore, Baeyer–Villiger oxidations are indispensable for synthesizing esters from ketones.[15,24]

For preparative chemistry, the ideal peroxide would be inexpensive, easily accessible, reproducible in its composition, and soluble in organic solvents. It should be safe and stable at ambient temperatures on the shelf. Finally, a solid oxidizing agent would be desirable that can easily be administered.

Presently, aqueous H_2O_2 is the most ubiquitous oxidizing agent in academic labs, although it is not ideal. The main drawback is the abundance of water it delivers to the reaction mixture which can lead to unwanted secondary reactions. Additionally, in case the reagents are not water-soluble the oxidations have to be performed in a biphasic system, slowing rates and requiring phase separations later. Furthermore, commercial aqueous H_2O_2 contains a large amount of nitric acid as a stabilizer. Nevertheless, commercially available H_2O_2 degrades at unpredictable rates,[25] and has to be titrated[25a,b] prior to each application when exact amounts of active oxygen are needed. Aqueous H_2O_2 also decomposes quickly in the presence of metal ions like Fe^{3+}.[25c] Water-free formulations of H_2O_2, for example, urea hydrogen peroxide (UHP)[26] and peroxocarbonates[27] are in use. The main disadvantage is that the composition of these materials is not well defined. Furthermore, they are insoluble in organic solvents and hard to remove from reaction mixtures. Other approaches include encapsulated[28] and immobilized versions of H_2O_2,[29] and H_2O_2 adducts of metal complexes.[30,31] Peroxides like $(Me_3SiO)_2$ and $(CH_3)_2C(OO)$ (DMDO) are applied, but their synthesis and storage are problematic.[31,32]

Phosphine oxides are important, for example, because they are unwanted byproducts of phosphine chemistry[33] and catalysis.[33–37] They are also co-products of Wittig and Appel reactions and can be used to probe the surface acidities of oxide materials.[38] Currently phosphine oxides receive attention regarding the analysis and decomposition of warfare agents,[39] as flame retardants,[40] and synthetic intermediates and targets.[16,41]

Phosphine oxides readily form hydrogen bonds with diverse types of donors. Examples include hydrogen-bonding with phenols,[42,43] with naphthol,[44] sulfonic acids,[45] and water.[11,13,46] Phosphine oxides with hydrogen bonds to silanols, phenols, and even chloroform have recently been

Department of Chemistry, Texas A&M University, College Station, TX, 77842-3012, USA. E-mail: bluemel@tamu.edu

† Electronic supplementary information (ESI) available. CCDC 1898472–1898476, 1930449 and 1937469. For ESI and crystallographic data in CIF or other electronic format see DOI: 10.1039/c9dt03070k

characterized.[17] The potential of phosphine oxides as hydrogen bond acceptors has been studied theoretically,[47] also in combination with hydrogen-bonded H_2O_2.[48]

Furthermore, the influence of hydrogen bonding on the ^{31}P solid-state NMR spectra of phosphine oxides has been analyzed in detail by our group[11–13,17,18] and Shenderovich.[49] When solid phosphine oxides are combined with porous materials, such as silica,[50] they adsorb on the surface by hydrogen-bonding with surface silanol groups, even in the absence of a solvent. This phenomenon and the dynamic properties have also been studied by multinuclear solid-state NMR.[13,18]

Recently, we discovered that phosphine oxides have the unique ability to stabilize hydrogen peroxide[11,12] and di(hydroperoxy)alkanes by forming strong hydrogen bonds.[12,14,15] The materials obtained exhibit general structural motifs for both adduct forms, the Hilliard adducts $(R_3PO{\cdot}H_2O_2)_2$,[11,12] and the Ahn adducts $R_3PO{\cdot}(HOO)_2CR'R''$ (R, R′, R″ = alkyl and aryl).[12,14,15] The peroxides are stabilized by well-defined hydrogen bonding by the phosphine oxides without compromising their oxidative efficiency. Both Hilliard and Ahn adducts selectively and instantaneously oxidize phosphines to phosphine oxides.[11,12,14,15] The merit of water-free oxidation in particular has been demonstrated by the clean synthesis of the water-sensitive diphosphine dioxide $Ph_2P(O)P(O)Ph_2$.[14] Sulfides are transformed selectively into sulfoxides in organic phases,[12,14] and Baeyer–Villiger oxidations of ketones are efficient with Hilliard and Ahn adducts.[15]

Both adduct types are safe and robust towards high temperatures and mechanical stress and have shelf lives of months at ambient temperatures.[11,12,14,15] The Hilliard and Ahn adducts do not contain acids or other impurities that would have to be removed, as in the case of aqueous H_2O_2, when it is needed for special applications.[51] Most importantly, the high solubility of all adducts in organic solvents allows for homogeneous oxidation reactions in one organic phase. The Hilliard and Ahn adducts are solid, have well-defined compositions, and they can easily be administered to reaction mixtures.

Because of the favorable characteristics of these useful and intrinsically interesting Hilliard and Ahn oxidizers we sought to further explore the scope of these phosphine oxide adducts. Regarding later applications on a larger scale, it is desirable to minimize the weight and cost of the solid oxidizers. In this respect the Hilliard adducts are more favorable than the Ahn adducts. Therefore, we focused on the former, also because the only structurally characterized Hilliard adducts reported so far are $(Cy_3PO{\cdot}H_2O_2)_2$,[11] $(^tBu_3PO{\cdot}H_2O_2)_2$,[12] $(Ph_3PO)_2{\cdot}H_2O_2$,[52] and $(Ph_3PO{\cdot}H_2O_2)_2{\cdot}H_2O_2$.[12] The Ph_3PO adducts have been the most elusive regarding a well-defined ratio of phosphine oxide to peroxide groups, although they are most desirable because the parent phosphine oxide is inexpensive and a waste product of the Wittig and Appel processes. In our quest to obtain highly soluble H_2O_2 adducts with well-defined composition, we turned to triarylphosphine oxides, incorporating methyl substituents in the *ortho* and *para* positions of the phenyl rings, as carriers for H_2O_2.

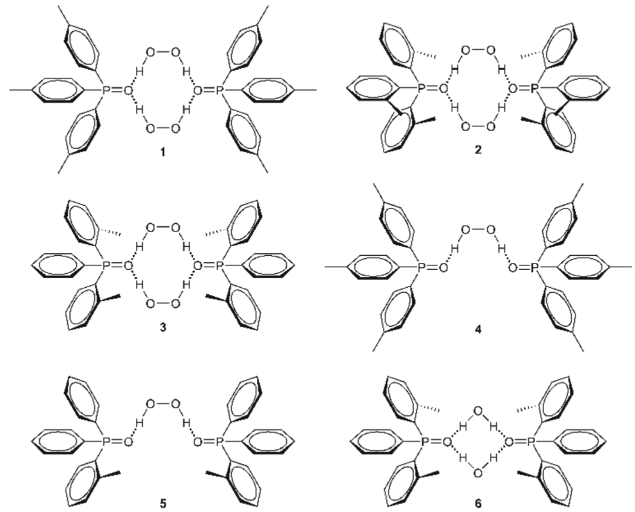

Scheme 1 The H_2O_2 adducts of triarylphosphine oxides **1–5** and the H_2O adduct **6**.

In this contribution we report five new H_2O_2 adducts of triarylphosphine oxides, **1–5**, and one H_2O adduct, **6** (Scheme 1). It is demonstrated that the adducts can be synthesized easily, reproducibly, and with the desired 1 : 1 or 2 : 1 ratio of phosphine oxide to peroxide groups. The adducts are fully characterized by single crystal X-ray diffraction, and two general structural motifs are identified. The ^{31}P, ^{13}C, and ^{1}H NMR data are analyzed and compared to the parent phosphine oxides. Due to the high solubility of all adducts, natural abundance ^{17}O NMR spectra are obtainable. The presence of the hydrogen-bonded H_2O_2 molecules is further confirmed by IR and Raman spectroscopy. The solubilities of the adducts in diverse organic solvents are quantified and the association of the adducts in solution is studied by Diffusion Ordered Spectroscopy (DOSY). The lifetimes of the adducts are monitored in solution at elevated temperatures.

2. Results and discussion

Synthesis and purification

In order to broaden the range of available hydrogen peroxide adducts and analytical methods for their characterization, the triarylphosphine oxide dimers **1–5** and the water adduct **6** have been synthesized (Scheme 1). The syntheses were straightforward by combining dichloromethane solutions of the corresponding phosphines with 35% aqueous hydrogen peroxide. After phase separation the adducts **1–3**, containing two H_2O_2 molecules per assembly, result. Additionally, **4**, incorporating only one H_2O_2 bridge per adduct, is isolated after heating a solution of **1** in toluene to 105 °C for 10 hours. Adduct **5** is obtained as the only product when the synthetic route used for **1–3** is applied. Interestingly, no mixed dimeric H_2O_2/H_2O adduct has been found in the solid state so far. Nevertheless, the existence of **4** and **5** suggests that the loss of active oxygen atoms in the adducts occurs in a stepwise manner, as described earlier for the di(hydroperoxy)alkane adducts of phosphine oxides.[15] The H_2O adduct **6** was obtained from **3** by decomposing the bound H_2O_2 with molecular sieves[11] and recrystallizing the product while exposed to the atmosphere.

For the comparison of spectroscopic data, the phosphine oxides corresponding to the adducts **1–6**, *p*-Tol_3PO (**7**), *o*-Tol_3PO (**8**), *o*-Tol_2PhPO (**9**), and *o*-$TolPh_2PO$ (**10**) have been synthesized.

The adducts **1–5** are mechanically and thermally stable and their melting points and ranges could be determined. The characterization of the adducts was furthermore facilitated by their readiness to crystallize in large habits with dimensions in the cm range (Fig. 1). Besides the single crystal X-ray structures, the IR and Raman spectroscopic data are reported. The ^{31}P NMR results are in agreement with earlier findings,[11,12] and the DOSY experiments elucidate the mono- *versus* dimeric nature of selected adducts in solution. Due to the high solubility of the adducts in organic solvents, the natural abundance ^{17}O NMR spectra could be obtained with well-resolved signals for the P═O and H_2O_2 oxygen nuclei.

X-Ray crystallography

All adducts **1–6** crystallize readily in large colorless specimens of high quality (Fig. 1). As earlier research on Ph_3PO as a crystallization aid for amines has shown,[53] the triarylphosphine oxide moieties are most probably responsible for the ease of crystallization. All adducts **1–6** have been investigated by single crystal X-ray diffraction. The structures are displayed in Fig. 2–8[54] and the P═O bond lengths, O⋯H and oxygen–oxygen distances O⋯H–O are summarized in Table 1.

The adducts **1–3** incorporate the H_2O_2 molecules sandwiched between the two P═O groups. The center of the assemblies contains the two H_2O_2 molecules in the characteristic chair conformation. The latter has been found earlier for the only other structurally characterized adducts with $(H_2O_2)_2$ cores, $(Cy_3PO·H_2O_2)_2$,[11] $(^tBu_3PO·H_2O_2)_2$,[12] and $(Ph_3PO·H_2O_2)_2·H_2O_2$.[12] The H_2O_2 molecules hydrogen-bonded in **1–3** feature dihedral angles defined by the H–O–O–H [═O⋯O–O⋯O═] angles of 99.042(12)° [89.060(11)°] (**1**), 100.003(18)° [100.069(18)°] (**2**), and 99.277(4)° [98.969(4)°] (**3**), which are considerably larger than the value of 90.2(6)° found in solid H_2O_2. The dihedral angles in the mono-H_2O_2 adducts

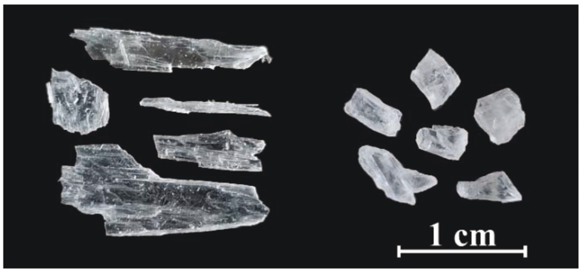

Fig. 1 Single crystals of **1** (left) and **2** (right).

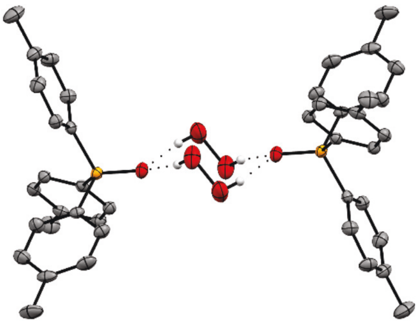

Fig. 2 Single crystal X-ray structure of (*p*-$Tol_3PO·H_2O_2)_2$ (**1**).[54]

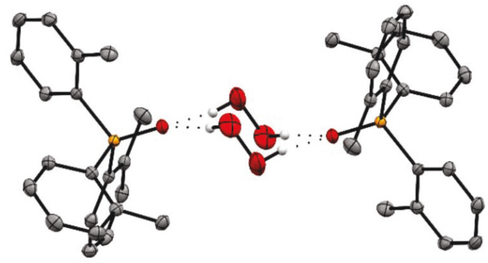

Fig. 3 Single crystal X-ray structure of (*o*-$Tol_3PO·H_2O_2)_2$ (**2**).[54]

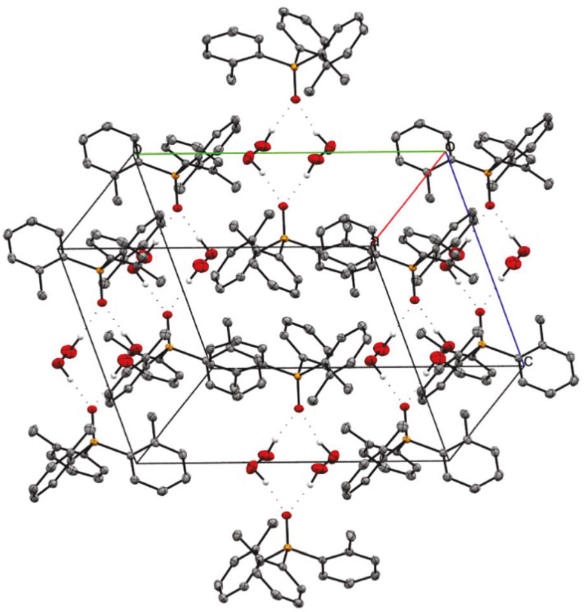

Fig. 4 Unit cell of the adduct (*o*-$Tol_3PO·H_2O_2)_2$ (**2**).[54]

4 and **5** are even larger with 131.868(4)° [93.062(5)°] (**4**) and 111.642(6)° [109.300(6)°] (**5**), most probably due to the steric demands of packing in the unit cell.

Although in **1** there appears to be additional space between the two phosphine oxide carrier molecules (Fig. 2), it is not used to incorporate a third H_2O_2 molecule, as found earlier for the triphenylphosphine oxide adduct $(Ph_3PO·H_2O_2)_2·H_2O_2$.[12]

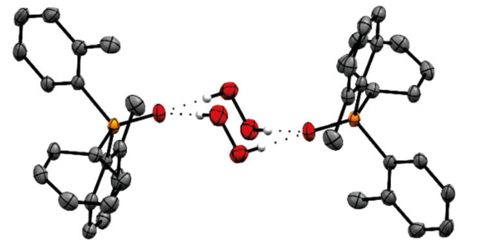

Fig. 5 Single crystal X-ray structure of (o-$Tol_2PhPO{\cdot}H_2O_2)_2$ (**3**).[54]

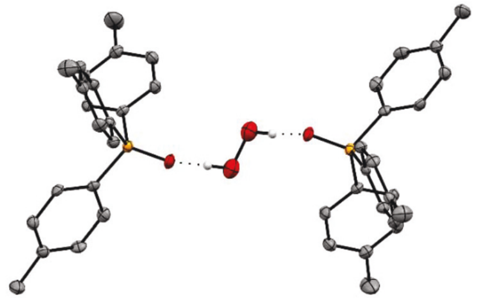

Fig. 6 Single crystal X-ray structure of (p-$Tol_3PO)_2{\cdot}H_2O_2$ (**4**).[54]

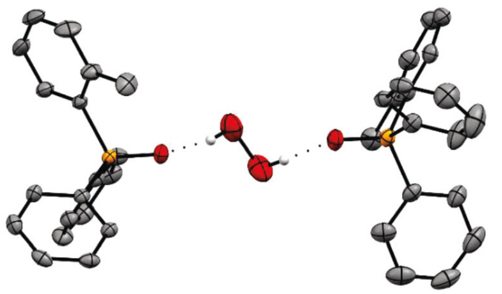

Fig. 7 Single crystal X-ray structure of (o-$TolPh_2PO)_2{\cdot}H_2O_2$ (**5**).[54]

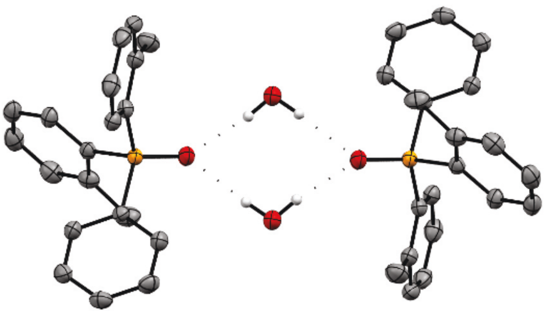

Fig. 8 Single crystal X-ray structure of (o-$Tol_2PhPO_2{\cdot}H_2O)_2$ (**6**).[54]

The available free space on one side of the dimeric assembly in **1** amounts to *ca.* 68 Å^3. This pocket size was estimated as the product of the distances ***a***, ***b***, and ***c*** with the following descriptions. ***a*** represents the minimal clearance between the *p*-Tol substituents of two different phosphine oxides in the dimeric assembly. ***b*** is double the maximal height of the chair formed by the two H_2O_2 molecules and the two P=O oxygen atoms. ***c*** has been defined as the distance between two mirrored oxygen atoms of the two different H_2O_2 molecules within one dimeric assembly. The available space estimated in this way seems large, however, part of this space is taken up by the CH_3 group of the *p*-Tol substituent of a neighboring dimeric assembly. Due to the hydrogen bond formation, the P=O bond order is reduced and the bond is weakened. The P=O bond is longer in **1** (1.4988(3) Å)[54] than in the parent phosphine oxide *p*-Tol_3PO (**7**) (1.4885(17) Å).[54]

Table 1 P=O bond lengths (Å), as well as O⋯H and oxygen–oxygen distances O⋯H–O (Å) of the adducts **1–6**[54]

Adduct	P=O bond length (Å)	O⋯H distance (Å)	O⋯H–O distance (Å)
1	1.4988(3)	1.9365(3)/1.9258(4)[a]	2.7734(4)/2.7651(5)[a]
2	1.5010(3)	1.8228(3)/1.8815(3)	2.7287(4)/2.8186(4)
3	1.50455(7)	1.91259(6)/1.84216(6)[a]	2.76245(8)/2.69200(9)[a]
4	1.49474(8)	1.92746(9)	2.72339(12)
5	1.4975(3)/ 1.4980(3)	1.8478(5)/1.8706(6)[a]	2.6844(8)/2.7202(8)[a]
6	1.488(16)	2.0032(16)/2.0504(16)	2.861(3)/2.915(3)

[a] Metrics from the major component of the disordered H_2O_2 are reported.

Regarding the X-ray structure of **2** (Fig. 3), it is obvious that the three methyl groups in the *ortho* positions of the phenyl substituents at phosphorus fill more of the space in the immediate surroundings of the two H_2O_2 molecules than the *para*-methyl-substituted phenyl groups in **1** or the unsubstituted phenyl groups in $(Ph_3PO{\cdot}H_2O_2)_2{\cdot}H_2O_2$.[12] However, contemplating only one dimeric assembly, there would still be room for a third H_2O_2 molecule. Estimating the free space in analogy to the procedure outlined above for **1**, *ca.* 35 Å^3 are obtained, which is about half the value for **1**. The distance ***a*** has the highest impact on the calculation, due to the presence of the *ortho* methyl groups in the *o*-Tol substituents. While the available space alone is still compatible with accommodating one more H_2O_2, the packing in the crystal is not favorable for a third H_2O_2 molecule per assembly. The unit cell of **2** (Fig. 4) displays the arrangement of the dimeric adducts in the crystal lattice. The dense packing of the assemblies and the particular arrangement of the adducts clearly does not facilitate the accommodation of a third H_2O_2 molecule.

The P=O bond in **2** is again elongated (1.5010(3) Å, Table 1) as compared with the phosphine oxide *o*-Tol_3PO (**8**) (1.478(2)/1.481(2) Å).[55] The lengthening of the P=O bond is more substantial (0.020/0.023 Å) than for **1**, so the *ortho* methyl substituents at the phenyl groups clearly have an impact.

In the X-ray structure of **3** (Fig. 5) the two methyl groups in the *ortho* positions of the phenyl substituents at phosphorus fill some of the space around the $(H_2O_2)_2$ core of the assembly. The center of the adducts again assumes the preferred chair conformation, which emerges as the general structural characteristic of all Hilliard H_2O_2 adducts of phosphine oxides with the dimeric motif $(R_3PO{\cdot}H_2O_2)_2$.

Adduct **4** has only half the number of active oxygen atoms as compared to **1–3**. It could be isolated as an intermediate in the stepwise release of oxygen when **1** was exposed to elevated temperatures in solution. Therefore, it might become useful as a more robust and mild oxidizer.

Curiously, the water molecule that is created when **1** loses one active oxygen atom has not been found in the crystal structure. Since adducts with a $(H_2O)_2$ core, like **6** (Scheme 1) exist, we assume that the structure of the mixed adduct (p-Tol_3PO)·(H_2O/H_2O_2)·(p-Tol_3PO) is not favorable for crystallization. The fact that the mono-H_2O_2 adduct **4** is preferred over the mono-H_2O adduct corroborates the finding that H_2O_2 is more firmly bound than a water molecule and replaces hydrogen-bonded water from phosphine oxides.[14] In this case, there would be space left for one water molecule, but the packing in the unit cell might prevent its incorporation in the structure. The P═O bond in **4** is lengthened from 1.4885(17) Å for p-Tol_3PO (**7**) to 1.49474(8) Å (Table 1). The difference in the bond lengths is only about 0.006 Å, illustrating the diminished effect of only one hydrogen-bonded H_2O_2 in the adduct on the P═O groups of **4**.

The single crystal X-ray structure of **5** resembles that of **4**, exhibiting the same structural motif $(R_3PO)_2{\cdot}H_2O_2$. The P═O bond lengths (Table 1) is slightly larger in **5**, while the O⋯H distance is correspondingly shorter.

The phosphine oxide hydrate **6** shows the high affinity of phosphine oxides for water[11,13] and is the first triarylphosphine oxide water adduct with the structural motif $(R_3PO{\cdot}H_2O)_2$ described so far (Fig. 8). Only the hemihydrate (p-$Tol_3PO)_2{\cdot}H_2O$ has been reported previously.[56] The other structurally characterized hydrate, $(Cy_3PO{\cdot}H_2O)_2$, incorporates a trialkylphosphine oxide.[13]

The four oxygen atoms per assembly of **6** lie in a plane (Fig. 8). The P═O bond of **6** is the shortest among the adducts **1–6**, and it can be concluded that the hydrogen bonding of the P═O groups to H_2O is weaker than the bonding to H_2O_2. The H–O–H angle amounts to 104.6°.

All O⋯H distances in **1–5** confirm the presence of hydrogen bonding, as they are within the range of 1.8228(3)–1.9365(3) Å (Table 1).[57] Hydrogen bonds typically exhibit O⋯H distances of 1.85 to 1.95 Å.[57] The H_2O adduct **6** shows slightly longer O⋯H distances, but the structure nevertheless suggests the presence of hydrogen bonds (Fig. 8). Furthermore, the O⋯H–O distances of **1–5**, which are another indicator for the formation of hydrogen bonds,[58] all lie within the range of 2.6844(8)–2.8186(4) Å (Table 1). This confirms strong hydrogen bonding, as the values are between 2.75 and 2.85 Å.[58] Only for the H_2O adduct **6**, the O⋯H–O distances of 2.861(3)/2.915(3) Å are slightly larger, but the visual impression of the presence of hydrogen bonds again dominates.

DOSY NMR spectroscopy

As the preceding section and the single crystal X-ray structures show, in the solid state the adducts **1–5** consist of dimers that are held together by hydrogen bonds. However, no information about the dissociation in different solvents is available at this time. Since Hilliard adducts can be transformed into Ahn adducts by exchange of H_2O_2 with $(HOO)_2CR_2$,[14] it is assumed that a certain degree of dissociation of the dimers $(R_3PO{\cdot}H_2O_2)_2$ takes place in solution. To clarify this issue, we sought to employ Diffusion-Ordered NMR Spectroscopy (DOSY) to probe the hydrogen bond association in **1–5**.[59] The phosphine oxide carriers of the adducts provide access to the straightforward ^{31}P DOSY experiments.[60,61] The resulting values should be within a ±1 Å error margin. The obtained Stokes diameters of the adducts and their corresponding phosphine oxides were compared with the maximal sizes of the species, as defined by the largest H⋯H distance within one molecule or assembly in the X-ray structure (Table 2). The reliability of the measurements is corroborated by the fact that the Stokes diameters of the adduct-free phosphine oxides correspond very well to the sizes calculated from their structures. This also confirms that there is no association between the phosphine oxides. Next, we sought to apply the method to the most stable Hilliard adduct[11] with a trialkylphosphine oxide carrier. For $(Cy_3PO{\cdot}H_2O_2)_2$ [11] in THF, a Stokes diameter of 18 Å was obtained. This corresponds well to the maximal H⋯H distance of 16.9 Å within the error margin of the DOSY measurement. Therefore, one can conclude qualitatively that this adduct undergoes only minimal dissociation in THF and remains mainly dimeric.

For the adducts with triarylphosphine oxide carriers **1–5**, however, the Stokes diameters are more in the range of the phosphine oxides (Table 2). In order to exclude that the polar solvent THF led to the dissociation of the dimeric adducts, the DOSY experiments were also performed using benzene and toluene. Nevertheless, only a marginal increase of the Stokes diameters of the adducts, as compared to their corresponding phosphine oxides, was found. Therefore, it is concluded on a qualitative basis that the adducts **1–5**, incorporating triarylphosphine oxide carriers, undergo dissociation in solution. Since the Stokes diameters of the adducts are still 1 to 2 Å larger than the values for the phosphine oxides, it is assumed that the dissociation of the dimers leads to the monomeric adducts of the type $R_3PO{\cdot}H_2O_2$. In a monomeric adduct the H_2O_2 mole-

Table 2 Stokes diameters obtained from DOSY measurements in C_6D_6 (*THF-d_8, #Tol-d_8), and maximal H⋯H distances of the adducts and their corresponding phosphine oxides, derived from the single crystal X-ray structures

	Stokes diameter [Å]		Maximal H⋯H distance [Å]	
Adduct	R_3PO	Adduct	R_3PO	Adduct
$(Cy_3PO{\cdot}H_2O_2)_2$ [11]	11*	18*	10.066	16.911 (ref. 11)
1	10*	9* 11 12#	11.277	17.938
2	10*	11	9.503	16.355
3	11	11	9.610	16.932
4	10	11	11.277	18.849
5	10	10	9.479	16.013

cule is "dangling" at the P═O oxygen atom and has a high degree of freedom regarding its motions without compromising the strength of the hydrogen bond. It can, for example, fold towards the substituents at phosphorus and in this way the size of the assembly is minimized. Therefore, the Stokes diameter of a monomeric adduct is only slightly larger than that of the phosphine oxide. The assumption that the adducts do not completely dissociate into R_3PO and H_2O_2 is also corroborated by the fact that the adducts show much higher solubility in most organic solvents than the parent phosphine oxides. In order to quantify the strength of the hydrogen bonding between H_2O_2 and the phosphine oxides, and the dissociation constant, more sophisticated techniques would be needed. These include, for example, theoretical calculations, as performed for N–H⋯N hydrogen-bonded systems,[62] and measurements at ultra-low temperatures, like those applied to cyclic trimers of phosphinic acids.[63] However, additional qualitative support for the presence of associated monomers of the type $R_3PO·H_2O_2$ described in this work, comes from ^{31}P and ^{17}O NMR, as outlined in the following sections.

^{31}P NMR spectroscopy

Due to the high solubility of the H_2O_2 adducts of the phosphine oxides in organic solvents (see below), ^{31}P NMR spectra can be recorded in short periods of time. For precise referencing, a capillary with liquid $ClPPh_2$ as the standard was centered in the NMR tubes. The changes of the ^{31}P chemical shifts of the adducts **1–6**, as compared with the corresponding phosphine oxides **7–10** are noticeable (Table 3). This result corroborates the assumption that in solution monomeric adducts of the type $R_3PO·H_2O_2$ are still present, and that the H_2O_2 does not entirely dissociate from the phosphine oxide carriers. The observable trend is that the formation of the hydrogen bond leads to deshielding of the ^{31}P nuclei due to electron density being relocated towards the oxygen atom in the P═O group. Therefore, the chemical shift values are generally higher for the adducts than for the phosphine oxides.

In contrast to the ^{31}P chemical shifts, there are only minimal changes in the ^{1}H and ^{13}C NMR data when creating the H_2O_2 adduct from a phosphine oxide. This can, for example, be seen when comparing the $\delta(^{13}C)$ and $J(^{31}P–^{13}C)$ values of **2** with those of **8**.[64]

Table 3 ^{31}P NMR chemical shifts of the adducts **1–6** and their corresponding phosphine oxides **7–10** in $CDCl_3$ and the differences of the chemical shift values

Adduct	$\delta(^{31}P)$ of adducts [ppm]	R_3PO	$\delta(^{31}P)$ of R_3PO [ppm]	$\Delta\delta(^{31}P)$ [ppm]
1	30.44	**7**	29.28	1.16
2	37.90	**8**	37.51	0.39
3	36.47	**9**	34.66	1.81
4	30.47	**7**	29.28	1.19
5	33.50	**10**	31.42	2.08
6	34.96	**9**	34.66	0.30

^{17}O NMR spectroscopy

While ^{31}P NMR spectroscopy is a routine method, ^{17}O NMR poses some challenges. The Larmor frequency of ^{17}O is in a favorable range, but its natural abundance is only 0.037%, which is about half of the value for ^{2}H. ^{17}O is a quadrupolar nucleus with a nuclear spin of I = 5/2. The quadrupole moment $Q = -2.6 \times 10^{-26}$ is of moderate size,[65] and therefore ^{17}O NMR signals can be expected to be broader than 100 Hz for species with unsymmetric electronic surroundings of the ^{17}O nucleus. Most ^{17}O NMR studies have been performed using isotopically enriched samples to facilitate the measurements. Examples include investigations of organic peroxides[66–68] and alkyl hydrotrioxides.[69] Furthermore, the peroxide binding to the active center of an enzyme[70] and polymer degradation mechanisms have been studied using ^{17}O NMR.[71] Enriched samples were also used for ^{17}O solid-state NMR investigations of hydrogen bonding in carboxylic acids,[72] and for studying polymorphs of triphenylphosphine oxide.[73]

However, due to the fast quadrupolar relaxation, transients can be collected in rapid succession and compounds with sufficient solubility in non viscous solvents are accessible to ^{17}O NMR in natural abundance, without isotopic enrichment. Fortunately, the adducts **1–6** are very soluble in organic solvents (see below). Especially their high solubility in CH_2Cl_2 is favorable because it allows the measurement of very concentrated samples in a non viscous solvent. The low viscosity of CH_2Cl_2 reduces the correlation time of the adducts and therefore diminishes the halfwidths of the quadrupolar ^{17}O NMR signals.[65]

A representative ^{17}O NMR spectrum is shown in Fig. 9 and all ^{17}O NMR data of the H_2O_2 adducts **1–5**, the H_2O adduct **6**, and the corresponding phosphine oxides **7–10** are summarized in Table 4. The spectrum in Fig. 9 shows the clearly resolved signals of **2** due to the large chemical shift dispersion of ^{17}O. The hydrogen-bonded H_2O_2 resonates at 184.32 ppm, the P═O oxygen nucleus at 60.04 ppm. The signal at −5.05 ppm corresponds to H_2O hydrogen-bonded to the P═O group. It came into existence in the course of the measurement due to slow decomposition of the H_2O_2 at the elevated temperature of 35 °C, which was applied in order to reduce the viscosity of the solution and therewith the correlation time and linewidth.[65]

The $\delta(^{17}O)$ of the P═O groups are found within the range of 45.83 to 60.04 ppm, in accordance with other compounds incorporating phosphorus–oxygen double bonds.[74] As com-

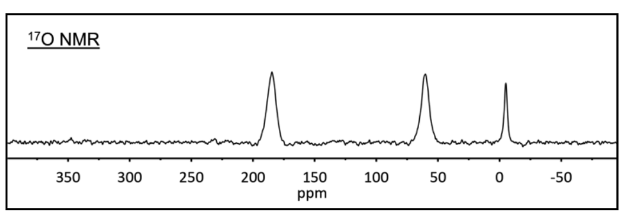

Fig. 9 ^{17}O NMR spectrum of $(o\text{-}Tol_3PO·H_2O_2)_2$ (**2**) in CH_2Cl_2, recorded at 35 °C.

Table 4 ^{17}O NMR chemical shifts $\delta(^{17}O)$ (signal halfwidths $\Delta\nu_{1/2}$ [Hz]) of the adducts **1–6** and their corresponding phosphine oxides **7–10** in CH_2Cl_2

Adduct	$\delta(^{17}O)$ [ppm] of bound H_2O_2/H_2O ($\Delta\nu_{1/2}$ [Hz])	$\delta(^{17}O)$ [ppm] of P=O group ($\Delta\nu_{1/2}$ [Hz])		$\delta(^{17}O)$ [ppm] of R_3PO ($\Delta\nu_{1/2}$ [Hz])
1	183.96 (494)	46.60 (365)	**7**	48.10 (434)
2	184.32 (548)	60.04 (429)	**8**	61.84 (517)
3	184.97 (253)	53.05 (302)	**9**	59.96 (125)[a]
4	184.77 (480)	45.83 (483)	**7**	48.10 (434)
5	184.23 (462)	46.22 (407)	**10**	48.99 (231)[b]
6	−6.69 (81.8)[a]	59.74 (284.4)[a]	**9**	59.96 (125)[a]

[a] The species **6** and **9** were not sufficiently soluble in CH_2Cl_2 and were therefore measured in acetonitrile at 75 °C. The signal of **9** is split into a doublet with $^1J(^{31}P–^{17}O)$ = 159.6 Hz. [b] $^1J(^{31}P–^{17}O)$ = 163.5 Hz.

pared to the $\delta(^{17}O)$ of the P=O group of **1** (46.60 ppm) (Table 4) the chemical shift for the oxygen nucleus of $Ph_3P{=}O$ in $CDCl_3$ has been reported as 43.3 ppm.[75] The deviation from this value and in general the variation of the $\delta(^{17}O)$ for the P=O groups in **1–6** and **7–10** reflects the presence of substituents at the aromatic rings. Furthermore, the solvent dependence of ^{17}O NMR chemical shifts can be substantial.[68]

Regarding the $\delta(^{17}O)$ of the P=O groups in the adducts **1–6** with those of the corresponding phosphine oxides **7–10** measured in the same solvents (excluding the pair **3**/**9**) shows that hydrogen bonding leads to a slight, but consistent upfield shift of the signals ranging from 0.22 (**6**/**9**) over 1.50 (**1**/**7**), 1.80 (**2**/**8**) and 2.27 (**4**/**7**), to 2.77 (**5**/**10**) ppm (Table 4). Obviously, the electron density around the oxygen nucleus is increased by the pull of electrons from the aromatic rings and phosphorus towards oxygen and the hydrogen bond. This leads to a shielding of ^{17}O and the observed upfield shift.

This result also corroborates the assumption that, although the DOSY measurements exclude dimeric assemblies of the adducts as present in the solids, the H_2O_2 is still associated with the phosphine oxides and monomeric assemblies of the type $R_3PO{\cdot}H_2O_2$ are prevalent in CH_2Cl_2 solution.

The solvent dependence of the halfwidths $\Delta\nu_{1/2}$ of the ^{17}O NMR signals is illustrated by the measurements of **6** and **9** in acetonitrile. The $\Delta\nu_{1/2}$ values are smaller when the measurements were performed in acetonitrile at 75 °C (Table 4). Under these conditions the halfwidth $\Delta\nu_{1/2}$ of the ^{17}O phosphine oxide resonance of **9** is small enough to reveal its splitting into a doublet with $^1J(^{31}P–^{17}O)$ = 159.6 Hz. This value is in accordance with the literature (160 Hz).[75] Acetonitrile and the elevated temperature of 75 °C were not used as a solvent for **1–5** due to concerns that it could decompose the H_2O_2 adducts (see below) in the course of the measurements or compete with the P=O groups as a hydrogen acceptor for H_2O_2.[68]

The ^{17}O NMR resonances of the hydrogen-bonded H_2O_2 moieties of **1–5** are in the narrow range between 183.62 and 184.97 ppm (Table 4). Compared with the literature value of 180 ppm in different solvents,[67,70] all hydrogen-bonded H_2O_2 in the adducts experience a downfield shift between 3.62 and 4.97 ppm. Obviously, the hydrogen bonding reduces the electron density around the ^{17}O nuclei, leading to a deshielding and higher $\delta(^{17}O)$ values. This result again supports the assumption that the adducts persist in solution as monomers of the type $R_3PO{\cdot}H_2O_2$. For the H_2O adduct **6** (Table 4) and the H_2O liberated by the decomposition of H_2O_2 in **2** (Fig. 9), upfield shifts of −6.69 and −5.05 ppm as compared to pure water with $\delta(^{17}O)$ = 0 ppm, are observed. The reason for this is most probably that hydrogen bonding among water molecules reduces the electron density at the ^{17}O nucleus in H_2O more than the hydrogen bonding with a P=O group.

IR and Raman spectroscopy

The IR spectra[76] of the H_2O_2 adducts **1–5** and the parent phosphine oxides **7–10** corroborate the results from ^{31}P NMR spectroscopy (Table 5, Fig. 10). The stretching frequencies and therewith wavenumbers for the P=O groups are lower for **1–5** as compared to **7–10** because the hydrogen bonding with H_2O_2 weakens the double bond. The lower bond order means that less energy is required to excite the stretching mode of the bond in the adducts and therefore lower wavenumbers are observed. The differences $\Delta\nu$(P=O) are in the range of 8–27 cm^{-1}, in accordance with an earlier limited study of adducts with varying H_2O_2 content.[11]

The ν(O–H) stretching bands of the hydrogen-bonded H_2O_2 in **1–5** display wavenumbers of 3214 to 3271 cm^{-1} which can be clearly distinguished from potential water bands around 3400 cm^{-1}.[11,76] The hydrogen bonding of the H_2O_2 to the P=O group weakens the O–H bonds which leads to lower ν(O–H)

Table 5 IR stretching frequencies ν(P=O) [cm^{-1}] of the P=O groups of the H_2O_2 adducts **1–5** and comparison with their corresponding neat phosphine oxides **7–10** $\Delta\nu$(P=O) [cm^{-1}], ν(O–H) of hydrogen-bonded H_2O_2, and the Raman ν(O–O) stretching frequencies of the hydrogen-bonded H_2O_2

Adduct/phosphine oxide	ν(P=O) [cm^{-1}] of adduct/phosphine oxide	$\Delta\nu$(P=O) [cm^{-1}]	ν(O–H) of adducts [cm^{-1}]	ν(O–O) [cm^{-1}]
1/7	1170/1185	15	3214	868
2/8	1150/1158	8	3271	869
3/9	1149/1176	27	3286	877
4/7	1172/1185	13	3225	871
5/10	1168/1190	22	3261	871
6/9	1159/1176	17	3450	—

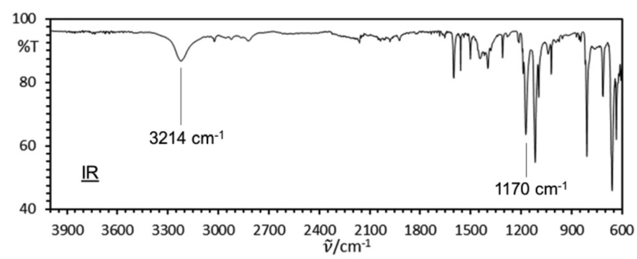

Fig. 10 IR spectrum of the neat H_2O_2 adduct ($(p\text{-Tol}_3PO{\cdot}H_2O_2)_2$ (**1**).

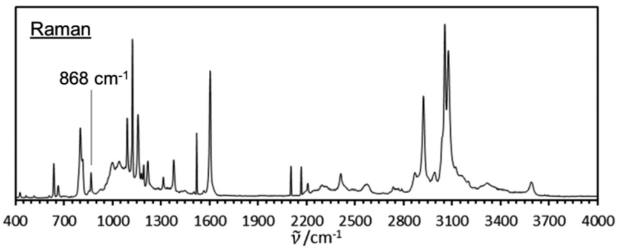

Fig. 11 Raman spectrum of the neat H_2O_2 adduct $(p\text{-}Tol_3PO{\cdot}H_2O_2)_2$ (**1**).

wavenumbers. In comparison, the water adduct **6** displays an O–H stretching band at 3450 cm^{-1}.

Due to the favorable symmetry of the adducts **1–5**, the Raman spectra showed the O–O stretching bands (Table 5). One representative Raman spectrum is displayed in Fig. 11. The ν(O–O) values are found within the narrow range from 868 to 877 cm^{-1}. They are in agreement with the theoretically predicted values for $(Ph_3PO{\cdot}H_2O_2)_2$.[48b] As expected, due to the bond order of one, the wavenumbers are much lower than those found for O_2 gas (1556 cm^{-1})[77] and O_2^- (1139 cm^{-1}).[78] Basically, the ν(O–O) for hydrogen-bonded H_2O_2 in **1–5** lies in between the values for aqueous (99.5%) H_2O_2 (880 cm^{-1})[79] and H_2O_2 vapor (864 cm^{-1}).[80] However, the O–O bonds in **1–5** are still stronger than those in alkali peroxides (736–790 cm^{-1})[81] or the popular oxidizing agent ^{t}BuOOH (847 cm^{-1}).[82]

Solubilities

The H_2O_2 adducts **1–5** are highly soluble in the most common organic solvents (Fig. 12). The quantified solubilities of **1–5** are highest in the protic solvents MeOH and EtOH. For example, more than 750 mg of **2** can be dissolved in one mL of MeOH. But even in $CHCl_3$ the solubilities are substantial. Overall, the solubilities in non protic solvents like THF or CH_2Cl_2 are highest for adducts containing *o*-Tol substituents at phosphorus, while they are in general lowest for those with only *p*-Tol groups. This is most probably due to the shielding of the polar H_2O_2 moieties by the methyl groups in the *ortho* positions, rendering the $R_3PO{\cdot}H_2O_2$ assemblies more hydrophobic. Curiously, all adducts are only sparingly soluble in water and hexane. This is, however, favorable with respect to isolating and purifying the adducts. After the biphasic synthesis the adducts are found in the organic phase. Large crystals can then be grown by overlaying this phase with hexane or pentane.

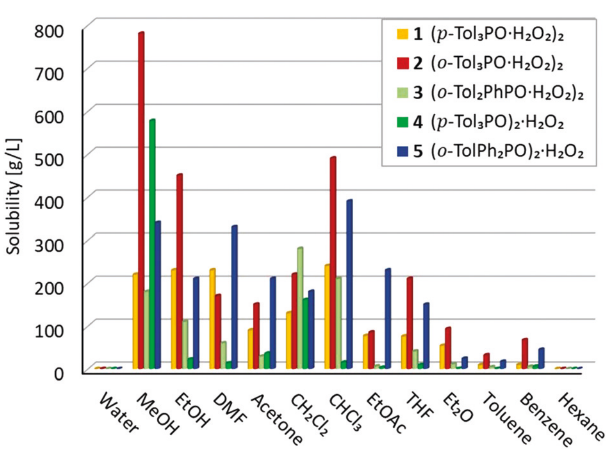

Fig. 12 Solubilities of the adducts **1–5** in representative solvents.

The high solubility of **1–5** in organic solvents can be exploited for many oxidation reactions. They can be performed in one organic phase, rendering a biphasic reaction mixture obsolete. This is especially advantageous in cases where the large amount of water that is introduced along with aqueous H_2O_2 would lead to unwanted secondary products. Having all educts dissolved in one phase also allows the reactions to proceed faster as compared to processes that only take place at phase boundaries. Naturally, no phase separation or cumbersome drying of the products is required when performing the reactions with **1–5** in organic solvents. The one water molecule formed per P═O group for **1–3** (per two P═O groups for **4** and **5**) when all peroxy groups have reacted remains hydrogen-bonded to the phosphine oxide carriers and will not interfere with the product or the progress of the reaction. The water adducts reported earlier[11,13] and adduct **6** (Scheme 1, Fig. 8) can be transformed into the corresponding H_2O_2 adducts by treating them with 35% aqueous H_2O_2. Therefore, after oxidation reactions, for example Baeyer Villiger, phosphine, or sulfide oxidations,[12,14,15] the phosphine oxides can easily be recharged by aqueous H_2O_2 after being removed from the reaction mixtures by precipitation with water or hexanes. Alternatively, the phosphine oxides can be bound to insoluble inorganic supports like silica[9a,34a] and separated from the supernatant reaction mixtures by decanting. After recharging with H_2O_2 the tethered phosphine oxides can be reused.

Shelf lives

The H_2O_2 adducts **1–5** are remarkably stable with respect to dry grinding and hammering. They do not react to sudden impact or release gas in a violent manner. Only when the powders are brought directly into a flame oxygen is released at slow speed without any pronounced audible or visual effect. Most of the adducts can even be molten without initial decomposition, while the oxygen effervesces in tiny bubbles at a higher temperature. It should be noted, however, that low pressure will eventually lead to loss of H_2O_2 from the phosphine oxide carrier. Consequently, lower yields of adducts are obtained, when prolonged vacuum is applied during the synthesis. On the other hand, combining Ph_3PO with aqueous H_2O_2 at 0 °C instead of ambient temperature, more than one H_2O_2 molecule per P═O group is incorporated in the adduct and $(Ph_3PO{\cdot}H_2O_2)_2{\cdot}H_2O_2$ is formed.[12]

The longevity of the adducts can be probed by determining their oxidative power. The latter can be monitored by a standardized *in situ* ^{31}P NMR test.[12,14] This test uses a weighed excess of Ph_3P that is converted into Ph_3PO by any peroxide group (but not by oxygen in the air), no matter whether it resides within the adducts **1–3** or the mono-H_2O_2 adducts **4** and **5**. The oxidative power, which corresponds to the number of active oxygen atoms

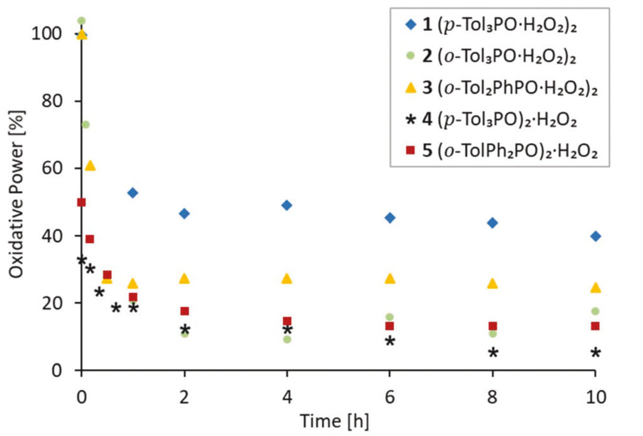

Fig. 13 Oxidative power of compounds **1–5** while being heated to 105 °C in toluene (**1–3**, **5**) or chlorobenzene (**4**).

in the sample, is then determined by the integrals of the ^{31}P NMR signals of Ph_3PO and Ph_3P. For $(p\text{-}Tol_3PO{\cdot}H_2O_2)_2$ (**1**), for example, 100% oxidative power corresponds to one active oxygen atom per P═O group. As solids, the adducts **1–5** remain oxidatively active over months at ambient temperature. For example, after three years of storage in the laboratory atmosphere at room temperature (22 °C), solid **1** retained 33% of its original oxidative power. After storing **1** for six months at −18 °C in a freezer, 91% of its oxidative power remained.

Due to the stability of the adducts, solutions of **1–3**, and **5** were heated to 105 °C in toluene, and aliquots were tested for oxidative power in the course of time (Fig. 13). Adduct **1** proved to be the most stable under these conditions, followed by **3**, while **2** and **5** are losing oxidative power more quickly and at about the same pace. Regarding adduct **1**, after 10 hours at 105 °C, more than half of its oxidative power was lost. The solvent toluene was then removed, the residue was redissolved in chlorobenzene and again heated to 105 °C while monitoring the oxidative power (Fig. 13, asterisks). Between the end of the first curve and the start of the curve using chlorobenzene there is a gap in oxidative power of about 5%, which is due to the vacuum being applied for removing toluene. Over the next 10 hours in chlorobenzene the oxidative power of the material was lost almost entirely. Since the persistence of about half of the original oxidative power of **1** suggested a stepwise loss of H_2O_2, with the second H_2O_2 being retained much longer, a separate experiment was conducted. Adduct **1** was heated to 105 °C for 10 hours, and subsequently the mono-H_2O_2 adduct **4** was identified and isolated in 76% yield. The fact that the oxygen loss of **4** was faster in chlorobenzene than in toluene speaks for the assumption that the decomposition of H_2O_2 in the adducts proceeds by a radical mechanism.

3. Conclusions

In order to investigate whether H_2O_2 adducts of triarylphosphine oxides can be obtained reproducibly with a common structural motif and a well-defined composition, five new hydrogen peroxide adducts of phosphine oxides have been synthesized and fully characterized, $(p\text{-}Tol_3PO{\cdot}H_2O_2)_2$ (**1**), $(o\text{-}Tol_3PO{\cdot}H_2O_2)_2$ (**2**), $(o\text{-}Tol_2PhPO{\cdot}H_2O_2)_2$ (**3**), $(p\text{-}Tol_3PO)_2{\cdot}H_2O_2$ (**4**), and $(o\text{-}TolPh_2PO)_2{\cdot}H_2O_2$ (**5**). For comparison of the analytical data, the water adduct $(o\text{-}Tol_2PhPO{\cdot}H_2O)_2$ (**6**) was obtained. The single crystal X-ray diffraction studies of **1–3** show that there is a common structural motif with two H_2O_2 moieties hydrogen-bound and bridging two phosphine oxide molecules. The same basic principle is observed for adduct **6**, with two H_2O molecules and two P═O groups constituting the core of the assembly, held together by hydrogen bonding. The adducts **4** and **5** each contain one H_2O_2 molecule sandwiched between two P═O groups and held in its place by hydrogen bonding.

DOSY spectroscopy revealed that the H_2O_2 adduct of a trialkylphosphine oxide, $(Cy_3PO{\cdot}H_2O_2)_2$, remains predominantly dimeric in solution, while the triarylphosphine oxide adducts **1–5** dissociate into monomeric adducts of the type $R_3PO{\cdot}H_2O_2$.

^{31}P NMR spectroscopy of the adducts **1–6**, in comparison with the corresponding parent phosphine oxides **7–10**, shows a downfield shift of the signals as the common trend. The hydrogen bonding of the P═O groups reduces the electron density around the ^{31}P nuclei, thus deshielding them. The solubilities of all adducts and phosphine oxides are very high in representative organic solvents and allow natural abundance ^{17}O NMR spectroscopy. The hydrogen bonding in the adducts leads to lower $\delta(^{17}O)$ values due to the shielding of the ^{17}O nuclei of the P═O groups as compared to the parent phosphine oxides. The ^{17}O NMR chemical shifts of the hydrogen-bonded H_2O_2 molecules, on the other hand, are higher than the value for H_2O_2 in aqueous solution. This result confirms that the hydrogen bonding of H_2O_2 to P═O groups is stronger than to H_2O molecules.

IR spectroscopy corroborates the NMR and X-ray crystallography results, as the P═O bonds are weakened in the adducts and therefore the stretching frequencies ν(P═O) are lowered as compared to those of the corresponding phosphine oxides. The ν(O–H) stretching frequencies of the bridging H_2O_2 moieties in **1–5** also display lower values than the water adduct **6**. Raman spectroscopy has allowed to determine the stretching frequencies of the O–O bonds of the hydrogen-bonded H_2O_2 molecules in **1–5**.

The decomposition of **1–5** has been monitored in toluene and chlorobenzene at elevated temperature. The adduct **1** is transformed into **4** within ten hours, indicating that the active oxygen of an adduct assembly is lost in a stepwise manner and that the mono-H_2O_2 adduct **4** is thermally more robust than **1**. However, in chlorobenzene all oxidative power is lost within ten hours at 105 °C.

In the context of previous studies from our group and others, this work highlights the immense structural diversity and interesting reactivity of the P═O···H arrangement. The stepwise loss of the active oxygen from the two H_2O_2 bridges of the phosphine oxide adducts and retention of the H_2O

molecules, in combination with the high solubility of the adducts, guarantee that the adducts will find applications, for example, as oxidizers in academic synthesis or as polymerization starters.

4. Experimental section

General considerations

All reactions were carried out using standard Schlenk line techniques and a purified N_2 atmosphere, if not stated otherwise. Reagents purchased from Sigma Aldrich or VWR were used without further purification. Aqueous H_2O_2 solution (35% w/w) was obtained from Acros Organics and used as received. Solvents were dried by boiling them over sodium, then they were distilled and stored under purified nitrogen. Acetone, dichloromethane (Aldrich, ACS reagent grade) and ethanol (200 proof) were dried over 3 Å molecular sieves (EMD Chemical Inc.) prior to use.

Solubility measurements of 1–5

The adducts (5 to 12 mg amounts) were placed into tared 20 mL vials. The desired solvent was added in dropsized portions while shaking the vial vigorously at 20 °C. Once all solid was dissolved, the overall weight gain was recorded, and the solvent volume was calculated.

NMR spectroscopy

The ^{1}H, ^{13}C, and ^{31}P NMR spectra were recorded at 499.70, 125.66, and 202.28 MHz on a 500 MHz Varian spectrometer. The ^{13}C and ^{31}P NMR spectra were recorded with ^{1}H decoupling if not stated otherwise. Neat Ph_2PCl ($\delta(^{31}P)$ = +81.92 ppm) in a capillary centered in the 5 mm NMR tubes was used for referencing the ^{31}P chemical shifts of dissolved compounds. For referencing the ^{1}H and ^{13}C chemical shifts the residual proton and the carbon signals of the solvents were used (C_6D_6: $\delta(^{1}H)$ = 7.16 ppm, $\delta(^{13}C)$ = 128.00 ppm; $CDCl_3$: $\delta(^{1}H)$ = 7.26 ppm, $\delta(^{13}C)$ = 77.00 ppm). The signal assignments are based on comparisons with analogous phosphine oxides[11–15,17] and $^{1}H,^{1}H$-COSY, $^{1}H,^{13}C$-HSQC, $^{1}H,^{13}C$-HMBC, and ^{31}P-decoupled NMR spectra. The assignments of all *o*-Tol substituent signals follows the numbering in the scheme provided under the Experimental description of **2**.

^{17}O NMR spectroscopy. The natural abundance ^{17}O NMR spectra were recorded using 0.3 to 0.5 molar CH_2Cl_2 solutions of the compounds at 35 °C. A Varian 500 NMR spectrometer equipped with a 5 mm broadband probe operating at 67.79 MHz was employed. The following measurement parameters have been optimized to yield spectra of good quality with 0.8×10^6 to 1.4×10^6 scans: spectral window (73.5 kHz), number of data points (7353), measurement pulse length (20 μs), pulse angle (90°), relaxation delay (30 ms), and acquisition time (100 ms). The chemical shifts were referenced externally using pure D_2O ($\delta(^{17}O)$ = 0 ppm).

^{31}P DOSY. The ^{31}P DOSY NMR measurements were performed using a Varian 500 NMR spectrometer equipped with a 5 mm broad band probe operating at 202.33 MHz. 0.01 to 0.02 molar solutions of the compounds in THF-d_8 were investigated at 25 °C. Hereby, 20 gradient increments were measured after optimizing the following parameters: diffusion gradient length (2.7 ms), diffusion delay (100 ms), spectral window (6.1 kHz), complex points (4096), measurement pulse length (12.65 μs), pulse angle (90°), relaxation delay (30 s), acquisition time (675 ms), number of scans (16), and number of steady state pulses (32).

IR spectroscopy

The IR spectra of the neat powders of all adducts and compounds were recorded with a Shimadzu IRAffinity-1 FTIR spectrometer equipped with a Pike Technologies MIRacle ATR plate.

Raman spectroscopy

The Raman spectra were acquired using a Jobin–Yvon Horiba Labram HR instrument coupled to an Olympus BX41 microscope with 514.51 nm laser excitation from an Ar-ion laser. A 600 lines per mm grating and an acquisition time of 2 s were applied. 60 scans gave spectra of good quality.

X-ray diffraction

See ESI.†

Synthesis and characterization of adducts

Tri-*p*-tolylphosphine oxide H_2O_2 adduct (p-$Tol_3PO\cdot H_2O_2)_2$ (1). *p*-Tol_3P (457 mg, 1.5 mmol) was placed in a Schlenk flask under a nitrogen atmosphere and dissolved in dichloromethane (5 mL). Under stirring 2.15 mL of aqueous hydrogen peroxide (35%, 25 mmol) were added to the solution. The mixture was stirred vigorously for 30 min, then the phases were separated, and the solvent was allowed to slowly evaporate from the organic phase at ambient temperature and pressure. A colorless powder was obtained. Recrystallization from dichloromethane (4 mL) and pentane (2 mL) by slow evaporation gave **1** in the form of a crystalline colorless solid (475 mg, 0.671 mmol, 89% yield). Melting range 142–146 °C.

NMR (δ, $CDCl_3$), $^{31}P\{^{1}H\}$ 30.44 (s); ^{1}H 8.09–7.79 (br s, O*H*), 7.53 (dd, $^{3}J(^{31}P–^{1}H)$ = 11.9 Hz, $^{3}J(^{1}H–^{1}H)$ = 8.0 Hz, 6H, H_o), 7.25 (dd, $^{3}J(^{1}H–^{1}H)$ = 8.0 Hz, $^{4}J(^{31}P–^{1}H)$ = 2.1 Hz, 6H, H_m), 2.39 (s, 9H, CH_3); ^{13}C 142.41 (d, $^{4}J(^{31}P–^{13}C)$ = 2.6 Hz, C_p), 132.16 (d, $^{2}J(^{31}P–^{13}C)$ = 10.3 Hz, C_o), 129.31 (d, $^{1}J(^{31}P–^{13}C)$ = 106.8 Hz, C_i), 129.28 (d, $^{3}J(^{31}P–^{13}C)$ = 12.5 Hz, C_m), 21.71 (d, $^{5}J(^{31}P–^{13}C)$ = 1.3 Hz, CH_3).

Tri-*o*-tolylphosphine oxide H_2O_2 adduct (o-$Tol_3PO\cdot H_2O_2)_2$ (2). *o*-Tol_3P (1.20 g, 3.94 mmol) was dissolved in dichloromethane (14 mL) in a Schlenk flask under ambient atmosphere and the solution was cooled to 0 °C. While stirring, 6.07 mL of aqueous hydrogen peroxide (35%, 71.0 mmol) were added. The reaction mixture was stirred vigorously for 1.5 h, while it slowly warmed up to 23 °C. The phases were separated, and the solvent was allowed to evaporate from the organic phase at ambient temperature and pressure. A colorless solid was obtained (1.363 g, 1.923 mmol, 98% yield). Melting range 134–137 °C.

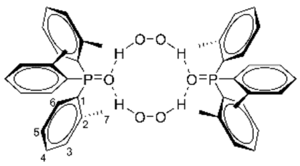

NMR (δ, $CDCl_3$), $^{31}P\{^1H\}$ 37.90 (s); ^1H 7.44 (tt, $^3J(^1H–^1H)$ = 7.5 Hz, $^5J(^{31}P–^1H)$ = $^4J(^1H–^1H)$ = 1.6 Hz, 3H, H4), 7.31 (ddquint, $^3J(^1H–^1H)$ = 7.5 Hz, $^4J(^{31}P–^1H)$ = 4.1 Hz, $^4J(^1H–^1H)$ = 0.8 Hz, 3H, H3), 7.15 (dt, $^3J(^1H–^1H)$ = 7.8 Hz, $^4J(^{31}P–^1H)$ = 2.7 Hz, 3H, H5), 7.09 (ddd, $^3J(^{31}P–^1H)$ = 14.0 Hz, $^3J(^1H–^1H)$ = 7.7 Hz, $^4J(^1H–^1H)$ = 1.5 Hz, 3H, H6), 6.86–6.59 (br s, OH), 2.48 (s, 9H, H7); ^{13}C 143.49 (d, $^2J(^{31}P–^{13}C)$ = 7.6 Hz, C2), 132.92 (d, $^2J(^{31}P–^{13}C)$ = 12.9 Hz, C6), 132.05 (d, $^3J(^{31}P–^{13}C)$ = 10.4 Hz, C3), 131.93 (d, $^4J(^{31}P–^{13}C)$ = 2.6 Hz, C4), 130.46 (d, $^1J(^{31}P–^{13}C)$ = 101.5 Hz, C1), 125.55 (d, $^3J(^{31}P–^{13}C)$ = 12.8 Hz, C5), 22.03 (d, $^3J(^{31}P–^{13}C)$ = 3.9 Hz, C7).

Di-*o*-tolylphenylphosphine oxide H_2O_2 adduct (*o*-$Tol_2PhPO·H_2O_2)_2$ (3). *o*-Tol_2PhP (232 mg, 0.8 mmol) was placed in a Schlenk flask and dissolved in dichloromethane (2.7 mL) under a nitrogen atmosphere. While stirring, 1.2 mL of aqueous hydrogen peroxide (35%, 14 mmol) were added. The mixture was stirred vigorously for 30 min, then the phases were separated, and the solvent was allowed to slowly evaporate from the organic phase at ambient temperature and pressure. Adduct **3** was obtained as a crystalline, slightly yellow solid (280 mg, 0.4 mmol, 100% yield). Mp 145 °C.

NMR (δ, $CDCl_3$), $^{31}P\{^1H\}$ 36.47 (s); ^1H 7.65–7.55 (m, 3H, H_o, H_p, Ph), 7.48 (dt, $^3J(^1H–^1H)$ = 7.6 Hz, $^4J(^{31}P–^1H)$ = 2.8 Hz, 2H, H_m, Ph), 7.44 (dt, $^3J(^1H–^1H)$ = 7.6 Hz, $^4J(^1H–^1H)$ = 0.9 Hz, 2H, H4), 7.31 (dd, $^3J(^1H–^1H)$ = 7.4 Hz, $^4J(^{31}P–^1H)$ = 4.1 Hz, 2H, H3), 7.15 (dt, $^3J(^1H–^1H)$ = 7.4 Hz, $^4J(^{31}P–^1H)$ = 2.5 Hz, 2H, H5), 7.02 (ddd, $^3J(^{31}P–^1H)$ = 13.9 Hz, $^3J(^1H–^1H)$ = 7.3 Hz, $^4J(^1H–^1H)$ = 0.9 Hz, 2H, H6), 5.98–5.60 (br s, 2H, OH), 2.50 (s, 6H, CH_3); ^{13}C 143.55 (d, $^2J(^{31}P–^{13}C)$ = 7.8 Hz, C2), 133.13 (d, $^2J(^{31}P–^{13}C)$ = 13.2 Hz, C6), 132.38 (d, $^2J(^{31}P–^{13}C)$ = 9.8 Hz, C_o, Ph), 132.25 (d, $^4J(^{31}P–^{13}C)$ = 2.6 Hz, C4), 132.17 (d, $^3J(^{31}P–^{13}C)$ = 10.4 Hz, C3), 132.08 (d, $^1J(^{31}P–^{13}C)$ = 103.3 Hz, C_i, Ph), 132.06 (d, $^4J(^{31}P–^{13}C)$ = 2.8 Hz, C_p, Ph), 130.27 (d, $^1J(^{31}P–^{13}C)$ = 103.1 Hz, C1), 128.73 (d, $^3J(^{31}P–^{13}C)$ = 12.1 Hz, C_m, Ph), 125.54 (d, $^3J(^{31}P–^{13}C)$ = 13.0 Hz, C5), 21.97 (d, $^3J(^{31}P–^{13}C)$ = 4.4 Hz, C7).

Tri-*p*-tolylphosphine oxide H_2O_2 adduct (*p*-$Tol_3PO)_2·H_2O_2$ (4). (*p*-$Tol_3PO·H_2O_2)_2$ (**1**) (514 mg, 0.725 mmol) was dissolved in toluene (30 mL). The solution was stirred and heated to 105 °C for 10 h. Subsequently, the oxidative power was determined by the method described earlier,[12] and found to be diminished to 55%. The solution was slowly cooled to −35 °C. Hereby, a colorless solid was obtained, which was redissolved in a mixture of dichloromethane and pentane (2 : 1, 10 mL). Slow evaporation of the solvents led to the formation of large colorless crystals of **4** (370.6 mg, 0.549 mmol, 76% yield). Melting range 116–137 °C.

NMR (δ, $CDCl_3$), $^{31}P\{^1H\}$ 30.47 (s); ^1H 7.54 (dd, $^3J(^{31}P–^1H)$ = 11.9 Hz, $^3J(^1H–^1H)$ = 8.1 Hz, 6H, H_o), 7.26 (dd, $^3J(^1H–^1H)$ = 7.8 Hz, $^4J(^{31}P–^1H)$ = 2.1 Hz, 6H, H_m), 6.84–6.46 (br s, O*H*), 2.40 (s, 9H, CH_3); ^{13}C 142.48 (d, $^4J(^{31}P–^{13}C)$ = 2.6 Hz, C_p), 132.22 (d, $^2J(^{31}P–^{13}C)$ = 10.4 Hz, C_o), 129.40 (d, $^1J(^{31}P–^{13}C)$ = 107.4 Hz, C_i), 129.33 (d, $^3J(^{31}P–^{13}C)$ = 12.6 Hz, C_m), 21.73 (d, $^5J(^{31}P–^{13}C)$ = 1.3 Hz, CH_3).

Diphenyl-*o*-tolylphosphine oxide H_2O_2 adduct (*o*-$TolPh_2PO)_2·H_2O_2$ (5). *o*-$TolPh_2P$ (221 mg, 0.8 mmol) was placed in a Schlenk flask and dissolved in dichloromethane (2.7 mL) under a nitrogen atmosphere. Under stirring 1.2 mL of aqueous hydrogen peroxide (35%, 14 mmol) were added to the solution. The mixture was stirred vigorously for 30 min before the phases were separated. Then the solvent was allowed to slowly evaporate from the organic phase at ambient temperature and pressure. Adduct **5** was obtained as a crystalline, slightly yellow solid (285 mg, 0.4 mmol, 100% yield). Melting range 129–132 °C.

NMR (δ, $CDCl_3$), $^{31}P\{^1H\}$ 33.50 (s); ^1H 7.64 (dd, $^3J(^{31}P–^1H)$ = 12.1 Hz, $^3J(^1H–^1H)$ = 6.9 Hz, 4H, H_o, Ph), 7.56 (tq, $^3J(^1H–^1H)$ = 7.3 Hz, $^5J(^{31}P–^1H) \approx {}^4J(^1H–^1H)$ = 1.4 Hz, 2H, H_p, Ph), 7.47 (dt, $^3J(^1H–^1H)$ = 7.6 Hz, $^4J(^{31}P–^1H)$ = 2.9 Hz, 4H, H_m, Ph), 7.43 (t, $^3J(^1H–^1H)$ = 7.5 Hz, 1H, H4, *o*-Tol), 7.29 (dd, $^3J(^1H–^1H)$ = 7.6 Hz, $^4J(^{31}P–^1H)$ = 4.2 Hz, 1H, H3, *o*-Tol), 7.14 (dt, $^3J(^1H–^1H)$ = 7.5 Hz, $^4J(^{31}P–^1H)$ = 2.2 Hz, 1H, H5, *o*-Tol), 7.01 (ddd, $^3J(^{31}P–^1H)$ = 14.2 Hz, $^3J(^1H–^1H)$ = 7.7 Hz, $^4J(^1H–^1H)$ = 1.4 Hz, 1H, H6, *o*-Tol) 2.44 (s, 6H, CH_3); ^{13}C 143.42 (d, $^2J(^{31}P–^{13}C)$ = 8.1 Hz, C2), 133.63 (d, $^2J(^{31}P–^{13}C)$ = 13.1 Hz, C6), 132.39 (d, $^4J(^{31}P–^{13}C)$ = 2.6 Hz, C4), 132.15 (d, $^1J(^{31}P–^{13}C)$ = 104.2 Hz, C_i, Ph), 132.06 (d, $^4J(^{31}P–^{13}C)$ = 2.8 Hz, C_p, Ph), 132.05 (d, $^3J(^{31}P–^{13}C)$ = 10.5 Hz, C3), 131.99 (d, $^2J(^{31}P–^{13}C)$ = 9.9 Hz, C_o, Ph), 130.24 (d, $^1J(^{31}P–^{13}C)$ = 104.0 Hz, C1), 128.72 (d, $^3J(^{31}P–^{13}C)$ = 12.2 Hz, C_m, Ph), 125.33 (d, $^3J(^{31}P–^{13}C)$ = 13.0 Hz, C5), 21.76 (d, $^3J(^{31}P–^{13}C)$ = 4.9 Hz, C7).

Di-*o*-tolylphenylphosphine oxide H_2O adduct (*o*-$Tol_2PhPO·H_2O)_2$ (6). (*o*-$Tol_2PhPO·H_2O_2)_2$ (**3**) (434 mg, 0.637 mmol) was placed in a Schlenk flask and dissolved in dichloromethane (30 mL). Dry molecular sieves (350 mg) were added and the mixture was stirred for 18 h at 20 °C. The molecular sieves were allowed to settle and the supernatant was collected with a syringe. The solvent was removed *in vacuo*. The colorless residue was recrystallized from toluene while being exposed to the atmosphere. The water adduct **6** was obtained as a crystalline colorless solid (340 mg, 0.524 mmol, 82% yield). Melting range 109–120 °C.

NMR (δ, $CDCl_3$), $^{31}P\{^1H\}$ 34.96 (s); ^1H 7.56–7.45 (m, 3H, H_o, H_p, Ph), 7.42–7.37 (m, 2H, H_m, Ph), 7.35 (t, $^3J(^1H–^1H)$ = 7.5 Hz, 2H, H4, *o*-Tol), 7.22 (dd, $^3J(^1H–^1H)$ = 7.7 Hz, $^4J(^{31}P–^1H)$ = 4.0 Hz, 2H, H3, *o*-Tol), 7.06 (dt, $^3J(^1H–^1H)$ = 7.5 Hz, $^4J(^{31}P–^1H)$ = 2.2 Hz, 2H, H5, *o*-Tol), 6.95 (ddd, $^3J(^{31}P–^1H)$ = 14.0 Hz, $^3J(^1H–^1H)$ = 7.7 Hz, $^4J(^1H–^1H)$ = 1.1 Hz, 2H, H6, *o*-Tol), 2.43 (s, 6H, CH_3); ^{13}C 143.54 (d, $^2J(^{31}P–^{13}C)$ = 7.8 Hz, C2), 133.08 (d, $^2J(^{31}P–^{13}C)$ = 12.9 Hz, C6), 132.75 (d, $^1J(^{31}P–^{13}C)$ = 102.9 Hz, C_i, Ph), 132.38 (d, $^2J(^{31}P–^{13}C)$ = 9.6 Hz, C_o, Ph), 132.12 (d, $^3J(^{31}P–^{13}C)$ = 10.3 Hz, C3) 132.05 (d, $^4J(^{31}P–^{13}C)$ = 2.6 Hz, C4), 131.87 (d, $^4J(^{31}P–^{13}C)$ = 2.8 Hz, C_p, Ph), 130.91 (d, $^1J(^{31}P–^{13}C)$ =

102.3 Hz, C1), 128.66 (d, $^3J(^{31}P-^{13}C)$ = 12.0 Hz, C_m, Ph), 125.48 (d, $^3J(^{31}P-^{13}C)$ = 12.9 Hz, C5), 21.99 (d, $^3J(^{31}P-^{13}C)$ = 4.4 Hz, C7).

Conflicts of interest

There are no conflicts of interest to declare.

Acknowledgements

This work was supported by the National Science Foundation (CHE-1300208 and CHE-1900100). We thank Dr Douglas Elliott for help with the DOSY measurements, Dr Diane Sellers for calibrating the Raman microscope, and Kyle J. Angle (REU) for measuring some solubilities.

Notes and references

1 (*a*) *Handbook of Advanced Methods and Processes in Oxidation Catalysis*, ed. D. Duprey and F. Cavani, Imperial College Press, 2014; (*b*) F. Cavani and J. H. Teles, *ChemSusChem*, 2009, **2**, 508–534; (*c*) Peroxides and Peroxide Compounds, in *Van Nostrand's Encyclopedia of Chemistry*, ed. A. E. Comyns, John Wiley & Sons, Inc., 2005.
2 Y. Lu, X. Zhao and S. Fang, *Foods*, 2019, **8**(31), 1–12.
3 H. Ying, Y. Yang, K. Cai and J. Cheng, *Eur. J. Org. Chem.*, 2019, 728–731.
4 Nobel Foundation, *The Nobel Prize in Physiology or Medicine 2015*, 2015.
5 (*a*) C. J. Legacy, A. Wang, B. J. O'Day and M. H. Emmert, *Angew. Chem., Int. Ed.*, 2015, **54**, 14907–14910; (*b*) C. J. Legacy and M. H. Emmert, *Synlett*, 2016, **27**, 1893–1897.
6 (*a*) P. C. B. Page, B. R. Buckley, C. Elliott, Y. Chan, N. Dreyfus and F. Marken, *Synlett*, 2016, **27**, 80–82; (*b*) D. Habibi, M. A. Zolfigol, M. Safaiee, A. Shamsian and A. Ghorbani-Choghamarani, *Catal. Commun.*, 2009, **10**, 1257–1260; (*c*) H. Golchoubian and F. Hosseinpoor, *Molecules*, 2007, **12**, 304–311; (*d*) M. Amini, M. Bagherzadeh, Z. Moradi-Shoeili, D. M. Boghaei, A. Ellern and L. K. Woo, *J. Coord. Chem.*, 2013, **66**, 464–472; (*e*) T. Okada, H. Matsumuro, S. Kitagawa, T. Iwai, K. Yamazaki, Y. Kinoshita, Y. Kimura and M. Kirihara, *Synlett*, 2015, **26**, 2547–2552; (*f*) J.-W. Chu and B. L. Trout, *J. Am. Chem. Soc.*, 2004, **126**, 900–908; (*g*) E. Wojaczyńska and J. Wojaczyński, *Chem. Rev.*, 2010, **110**, 4303–4356; (*h*) B. Zhang, S. Li, M. Cokoja, E. Herdtweck, J. Mink, S.-L. Zang, W. A. Herrmann and F. E. Kühn, *Z. Naturforsch., B: J. Chem. Sci.*, 2014, **69**, 1149–1163; (*i*) Y. Xie, Y. Li, S. Zhou, Y. Zhang, M. Chen and Z. Li, *Synlett*, 2018, **29**, 340–343.
7 (*a*) D. J. Covell and M. C. White, *Tetrahedron*, 2013, **69**, 7771–7778; (*b*) P. E. Gormisky and M. C. White, *J. Am. Chem. Soc.*, 2013, **135**, 14052–14055; (*c*) T. J. Osberger, D. C. Rogness, J. T. Kohrt, A. F. Stepan and M. C. White, *Nature*, 2016, **537**, 214–219; (*d*) J. M. Howell, K. Feng, J. R. Clark, L. J. Trzepkowski and M. C. White, *J. Am. Chem. Soc.*, 2015, **137**, 14590–14593; (*e*) B. H. Brodsky and J. Du Bois, *J. Am. Chem. Soc.*, 2005, **127**, 15391–15393.
8 (*a*) J. Hou, Y. Chen, B. Cordes, D. Ma, J. Wang, X. Wang, F. E. Kühn, H. Guo and M. D. Zhou, *Chem. Commun.*, 2015, **51**, 7439–7442; (*b*) M. D. Zhou, M. Liu, J. Huang, J. Zhang, J. Wang, X. Li, F. E. Kühn and S. L. Zang, *Green Chem.*, 2015, **17**, 1186–1193; (*c*) M. Drees, S. A. Hauser, M. Cokoja and F. E. Kühn, *J. Organomet. Chem.*, 2013, **748**, 36–45; (*d*) M. A. Goodman and M. R. Detty, *Synlett*, 2006, 1100–1104; (*e*) I. I. E. Markovits, W. A. Eger, S. Yue, M. Cokoja, C. J. Münchmeyer, B. Zhang, M.-D. Zhou, A. Genest, J. Mink, S.-L. Zang, N. Rösch and F. E. Kühn, *Chem. – Eur. J.*, 2013, **19**, 5972–5979; (*f*) H. Yao and D. E. Richardson, *J. Am. Chem. Soc.*, 2000, **122**, 3220–3221; (*g*) G. S. Owens and M. M. Abu-Omar, *Chem. Commun.*, 2000, 1165–1166.
9 (*a*) J. Blümel, *Inorg. Chem.*, 1994, **33**, 5050–5056; (*b*) J. Sommer, Y. Yang, D. Rambow and J. Blümel, *Inorg. Chem.*, 2004, **43**, 7561–7563.
10 T. Posset, F. Rominger and J. Blümel, *Chem. Mater.*, 2005, **17**, 586–595.
11 C. R. Hilliard, N. Bhuvanesh, J. A. Gladysz and J. Blümel, *Dalton Trans.*, 2012, **41**, 1742–1754.
12 S. H. Ahn, K. J. Cluff, N. Bhuvanesh and J. Blümel, *Angew. Chem., Int. Ed.*, 2015, **54**, 13341–13345, (*Angew. Chem.*, 2015, **127**, 13539–13543).
13 C. R. Hilliard, S. Kharel, K. J. Cluff, N. Bhuvanesh, J. A. Gladysz and J. Blümel, *Chem. – Eur. J.*, 2014, **20**, 17292–17295.
14 S. H. Ahn, N. Bhuvanesh and J. Blümel, *Chem. – Eur. J.*, 2017, **23**, 16998–17009.
15 S. H. Ahn, D. Lindhardt, N. Bhuvanesh and J. Blümel, *ACS Sustainable Chem. Eng.*, 2018, **6**, 6829–6840.
16 S. Kharel, T. Jia, N. Bhuvanesh, J. H. Reibenspies, J. Blümel and J. A. Gladysz, *Chem. – Asian J.*, 2018, **13**, 2632–2640.
17 S. Kharel, N. Bhuvanesh, J. A. Gladysz and J. Blümel, *Inorg. Chim. Acta*, 2019, **490**, 215–219.
18 S. Kharel, K. J. Cluff, N. Bhuvanesh, J. A. Gladysz and J. Blümel, *Chem. – Asian J.*, 2019, **14**, 2704–2711.
19 (*a*) D. W. Stephan, *Science*, 2016, **354**, 1248; (*b*) J. M. Bayne and D. W. Stephan, *Chem. Soc. Rev.*, 2016, **45**, 765–774.
20 M. Mehta, I. G. De la Arada, M. Perez, D. Porwal, M. Oestreich and D. W. Stephan, *Organometallics*, 2016, **35**, 1030–1035.
21 Z. S. Han, N. Goyal, M. A. Herbage, J. D. Sieber, B. Qu, Y. Xu, Z. Li, J. T. Reeves, J.-N. Desrosiers, S. Ma, N. Grinberg, H. Lee, H. P. R. Mangunuru, Y. Zhang, D. Krishnamurthy, B. Z. Lu, J. J. Song, G. Wang and C. H. Senanayake, *J. Am. Chem. Soc.*, 2013, **135**, 2474–2477.
22 (*a*) T. E. Barder and S. L. Buchwald, *J. Am. Chem. Soc.*, 2007, **129**, 5096–5101; (*b*) D. B. Copley, F. Fairbrother, J. R. Miller and A. Thompson, *Proc. Chem. Soc., London*, 1964, 300–301.
23 (*a*) X. Cai, S. Majumdar, G. C. Fortman, L. M. Frutos, M. Temprado, C. R. Clough, C. C. Cummins, M. E. Germain, T. Palluccio, E. V. Rybak-Akimova,

B. Captain and C. D. Hoff, *Inorg. Chem.*, 2011, **50**, 9620–9630; (*b*) A. Blake, G. McQuillan, I. Oxton and D. Troy, *J. Mol. Struct.*, 1982, **78**, 265–271; (*c*) J. E. Nycz and R. Musiol, *Heteroat. Chem.*, 2006, **17**, 310–316.

24 (*a*) M. Uyanik and K. Ishihara, *ACS Catal.*, 2013, **3**, 513–520; (*b*) L. Zhou, X. Liu, J. Ji, Y. Zhang, X. Hu, L. Lin and X. Feng, *J. Am. Chem. Soc.*, 2012, **134**, 17023–17026; (*c*) L. Zhou, X. Liu, J. Ji, Y. Zhang, W. Wu, Y. Liu, L. Lin and X. Feng, *Org. Lett.*, 2014, **16**, 2938–3941.

25 (*a*) N. V. Klassen, D. Marchington and H. C. E. McGowan, *Anal. Chem.*, 1994, **66**, 2921–2925; (*b*) Y. Cui, B. Zhang, B. Liu, H. Chen, G. Chen and D. Tang, *Microchim. Acta*, 2011, **174**, 137–144; (*c*) T. Tsuneda and T. Taketsugu, *Phys. Chem. Chem. Phys.*, 2018, **20**, 24992–24999.

26 (*a*) L. Ji, Y.-N. Wang, C. Qian and X.-Z. Chen, *Synth. Commun.*, 2013, **43**, 2256–2264; (*b*) D. Kaur and B. R. Chhabra, *J. Chem., Biol. Phys. Sci.*, 2013, **3**, 980–987; (*c*) M. C. Ball and S. Massey, *Thermochim. Acta*, 1995, **261**, 95–106; (*d*) J. A. Dobado, J. Molina and D. Portal, *J. Phys. Chem. A*, 1998, **102**, 778–784; (*e*) S. Taliansky, *Synlett*, 2005, 1962–1963; (*f*) M. S. Cooper, H. Heaney, A. J. Newbold and W. R. Sanderson, *Synlett*, 1990, 533–535.

27 (*a*) N. Koukabi, *Synlett*, 2010, 2969–2970; (*b*) A. McKillop and W. R. Sanderson, *J. Chem. Soc., Perkin Trans. 1*, 2000, 471–476; (*c*) D. P. Jones and W. P. Griffith, *J. Chem. Soc., Dalton Trans.*, 1980, 2526–2532.

28 S. Bednarz, B. Ryś and D. Bogdał, *Molecules*, 2012, **17**, 8068–8078.

29 (*a*) T. Jiang, W. Wang and B. Han, *New J. Chem.*, 2013, **37**, 1654–1664; (*b*) G. K. S. Prakash, A. Shakhmin, K. E. Glinton, S. Rao, T. Mathew and G. A. Olah, *Green Chem.*, 2014, **16**, 3616–3622.

30 (*a*) C. Mühle, E.-M. Peters and M. Jansen, *Z. Naturforsch., B: J. Chem. Sci.*, 2009, **64**, 111–115; (*b*) J. Cho, S. Jeon, S. A. Wilson, L. V. Liu, E. A. Kang, J. J. Braymer, M. H. Lim, B. Hedman, K. O. Hodgson, J. S. Valentine, E. I. Solomon and W. Nam, *Nature*, 2011, **478**, 502–505; (*c*) T. Schölkopf, N.-D. Van and T. Schleid, *Inorg. Chim. Acta*, 2011, **374**, 181–186; (*d*) A. Kunishita, J. D. Scanlon, H. Ishimaru, K. Honda, T. Ogura, M. Suzuki, C. J. Cramer and S. Itoh, *Inorg. Chem.*, 2008, **47**, 8222–8232; (*e*) M. Schulz, J. H. Teles, J. Sundermeyer and G. Wahl, *US Patent* 6054407, 2000.

31 K. Korth, A. Schorm, J. Sundermeyer, H. Hermann and G. Boche, Peroxo Complexes of Molybdenum, Tungsten and Rhenium with Phase Transfer Active Ligands: Catalysts for the Oxidation of Olefins and Aromatics by Hydrogen Peroxide and Bistrimethylsilyl Peroxide, in *Organosilicon Chemistry IV*, Wiley-VCH, Weinheim, 2000, pp. 238–244.

32 A. V. Arzumanyan, R. A. Novikov, A. O. Terent'ev, M. M. Platonov, V. G. Lakhtin, D. E. Arkhipov, A. A. Korlyukov, V. V. Chernyshev, A. N. Fitch, A. T. Zdvizhkov, I. B. Krylov, Y. V. Tomilov and G. I. Nikishin, *Organometallics*, 2014, **33**, 2230–2246, and refs. cited.

33 (*a*) M. Bogza, T. Oeser and J. Blümel, *J. Organomet. Chem.*, 2005, **690**, 3383–3389; (*b*) R. Fetouaki, A. Seifert, M. Bogza, T. Oeser and J. Blümel, *Inorg. Chim. Acta*, 2006, **359**, 4865–4873.

34 (*a*) J. Blümel, *Coord. Chem. Rev.*, 2008, **252**, 2410–2423; (*b*) J. Guenther, J. Reibenspies and J. Blümel, *Adv. Synth. Catal.*, 2011, **353**, 443–460; (*c*) R. Silbernagel, A. Diaz, E. Steffensmeier, A. Clearfield and J. Blümel, *J. Mol. Catal. A: Chem.*, 2014, **394**, 217–223; (*d*) C. Merckle and J. Blümel, *Adv. Synth. Catal.*, 2003, **345**, 584–588; (*e*) C. Merckle and J. Blümel, *Top. Catal.*, 2005, **34**, 5–15.

35 (*a*) J. H. Baker, N. Bhuvanesh and J. Blümel, *J. Organomet. Chem.*, 2017, **847**, 193–203; (*b*) Y. Yang, B. Beele and J. Blümel, *J. Am. Chem. Soc.*, 2008, **130**, 3771–3773; (*c*) B. Beele, J. Guenther, M. Perera, M. Stach, T. Oeser and J. Blümel, *New J. Chem.*, 2010, **34**, 2729–2731.

36 (*a*) J. C. Pope, T. Posset, N. Bhuvanesh and J. Blümel, *Organometallics*, 2014, **33**, 6750–6753; (*b*) T. Posset and J. Blümel, *J. Am. Chem. Soc.*, 2006, **128**, 8394–8395; (*c*) T. Posset, J. Guenther, J. Pope, T. Oeser and J. Blümel, *Chem. Commun.*, 2011, **47**, 2059–2061.

37 (*a*) S. Reinhard, P. Soba, F. Rominger and J. Blümel, *Adv. Synth. Catal.*, 2003, **345**, 589–602; (*b*) F. Piestert, R. Fetouaki, M. Bogza, T. Oeser and J. Blümel, *Chem. Commun.*, 2005, 1481–1483; (*c*) K. J. Cluff, N. Bhuvanesh and J. Blümel, *Chem. – Eur. J.*, 2015, **21**, 10138–10148; (*d*) S. Reinhard, K. D. Behringer and J. Blümel, *New J. Chem.*, 2003, **27**, 776–778.

38 (*a*) A. Zheng, S.-B. Liu and F. Deng, *Chem. Rev.*, 2017, **117**, 12475–12531; (*b*) R. Yerushalmi, J. C. Ho, Z. Fan and A. Javey, *Angew. Chem., Int. Ed.*, 2008, **47**, 4440–4442; (*c*) J. P. Osegovic and R. S. Drago, *J. Phys. Chem. B*, 2000, **104**, 147–154; (*d*) S. Hayashi, K. Jimura and N. Kojima, *Bull. Chem. Soc. Jpn.*, 2014, **87**, 69–75; (*e*) S. Machida, M. Sohmiya, Y. Ide and Y. Sugahara, *Langmuir*, 2018, **34**, 12694–12701.

39 (*a*) A. R. Wilmsmeyer, W. O. Gordon, E. D. Davis, B. A. Mantooth, T. A. Lalain and J. R. Morris, *Rev. Sci. Instrum.*, 2014, **85**, 014101; (*b*) J. Kemsley, *Chem. Eng. News*, 2014, **92**, 29.

40 (*a*) H. Ren, J. Sun, B. Wu and Y. Zhou, *Polym. Degrad. Stab.*, 2007, **92**, 956–961; (*b*) M. A. Espinosa, M. Galia and V. Cadiz, *J. Polym. Sci., Part A: Polym. Chem.*, 2004, **42**, 3516–3526.

41 (*a*) J. Chrzanowski, D. Krasowska and J. Drabowicz, *Heteroat. Chem.*, 2018, **29**, e21476; (*b*) T. Kovacs and G. Keglevich, *Curr. Org. Chem.*, 2017, **21**, 569–585; (*c*) D. Herault, D. H. Nguyen, D. Nuel and G. Buono, *Chem. Soc. Rev.*, 2015, **44**, 2508–2528; (*d*) M. D. Fletcher, *Organophosphorus Reagents*, 2004, 171–214; (*e*) H. R. Hays and D. J. Peterson, *Org. Phosphorus Compd.*, 1972, **3**, 341–500; (*f*) H. Adams, R. C. Collins, S. Jones and C. J. A. Warner, *Org. Lett.*, 2011, **13**, 6576–6579.

42 (*a*) D. Nunez-Villanueva and C. A. Hunter, *Chem. Sci.*, 2017, **8**, 206–213; (*b*) A. E. Stross, G. Iadevaia and C. A. Hunter, *Chem. Sci.*, 2016, **7**, 94–101; (*c*) G. Iadevaia, A. E. Stross,

A. Neumann and C. A. Hunter, *Chem. Sci.*, 2016, **7**, 1760–1767; (*d*) R. Cuypers, E. J. R. Sudhölter and H. Zuilhof, *ChemPhysChem*, 2010, **11**, 2230–2240.
43 N. A. Bewick, A. Arendt, Y. Li, S. Szafert, T. Lis, K. A. Wheeler, J. Young and R. Dembinski, *Curr. Org. Chem.*, 2015, **19**, 469–474.
44 S. J. Pike and C. A. Hunter, *Org. Biomol. Chem.*, 2017, **15**, 9603–9610.
45 N. J. Burke, A. D. Burrows, M. F. Mahon and J. E. Warren, *Inorg. Chim. Acta*, 2006, **359**, 3497–3506.
46 R. Joshi and S. P. Pasilis, *J. Mol. Liq.*, 2015, **209**, 381–386.
47 I. Alkorta and J. Elguero, *J. Phys. Chem. A*, 1999, **103**, 272–279.
48 (*a*) D. V. Ilyin, W. A. Goddard III, J. J. Oppenheim and T. Cheng, First-principles–based reaction kinetics from reactive molecular dynamics simulations: Application to hydrogen peroxide decomposition, *Proc. Natl. Acad. Sci. U. S. A.*, 2018, 1, 201701383, (*b*) T. Tsuneda, J. Miyake and K. Miyatake, *ACS Omega*, 2018, **3**, 259–265.
49 (*a*) E. Y. Tupikina, M. Bodensteiner, P. M. Tolstoy, G. S. Denisov and I. G. Shenderovich, *J. Phys. Chem. C*, 2018, **122**, 1711–1720; (*b*) G. Begimova, E. Y. Tupikina, V. K. Yu, G. S. Denisov, M. Bodensteiner and I. G. Shenderovich, *J. Phys. Chem. C*, 2016, **120**, 8717–8729.
50 K. R. Iler, *The Chemistry of Silica*, John Wiley, New York, 1979.
51 Q. Lin, Y. Jiang, J. Geng and Y. Qian, Removal of Organic Impurities with Activated Carbons for Ultra-Pure Hydrogen Peroxide Preparation, *Chem. Eng. J.*, 2008, **139**, 264–271.
52 D. Thierbach, F. Huber and H. Preut, *Acta Crystallogr., Sect. B: Struct. Crystallogr. Cryst. Chem.*, 1980, **36**, 974–977.
53 M. C. Etter and P. W. Baures, Triphenylphosphine Oxide as a Crystallization Aid, *J. Am. Chem. Soc.*, 1988, **110**, 639–640.
54 The following CCDC reference numbers contain the supplementary crystallographic data for the corresponding compounds **1–7** for this paper: 1898472 ((p-$Tol_3PO{\cdot}H_2O_2)_2$, **1**), 1898473 ((o-$Tol_3PO{\cdot}H_2O_2)_2$, **2**), 1898474 ((o-Tol_2PhPO $H_2O_2)_2$, **3**), 1898475 ((p-$Tol_3PO)_2{\cdot}H_2O_2$, **4**), 1898476 ((o-$TolPh_2PO)_2H_2O_2$, **5**), 1930449 ((o-Tol_2PhPO $H_2O)_2$, **6**), and 1937469 (p-Tol_3PO, **7**).†
55 F. R. Fronczek, CCDC 1021095, *CSD Communication*, 2014, DOI: 10.5517/cc138jkg.
56 M. R. Churchill, R. F. See, S. L. Randall and J. D. Atwood, *Acta Crystallogr., Sect. C: Cryst. Struct. Commun.*, 1993, **49**, 345–347.
57 G. A. Jeffrey, *An Introduction to Hydrogen Bonding*, Oxford University Press, Oxford, 1997.
58 E. N. Baker and R. E. Hubbard, Hydrogen Bonding in Globular Proteins, *Prog. Biophys. Mol. Biol.*, 1984, **44**, 97–179.
59 E. J. Cabrita and S. Berger, *Magn. Reson. Chem.*, 2001, **39**, S142–S148.
60 J. L. Cook, C. A. Hunter, C. M. R. Low, A. Perez-Velasco and J. G. Vinter, *Angew. Chem., Int. Ed.*, 2007, **46**, 3706–3709.
61 G. Kagan, W. Li, R. Hopson and P. G. Williard, *Org. Lett.*, 2009, **11**, 4818–4821.
62 (*a*) R. Pollice, M. Bot, I. J. Kobylianskii, I. Shederovich and P. Chen, *J. Am. Chem. Soc.*, 2017, **139**, 13126–13140; (*b*) R. Pollice, F. Fleckenstein, I. Shenderovich and P. Chen, *Angew. Chem., Int. Ed*, 2019, DOI: 10.1002/anie.201905436; (*c*) E. Y. Tupikina, M. Sigalov, I. G. Shenderovich, V. V. Mulloyarova, G. S. Denisov and P. M. Tolstoy, *J. Chem. Phys.*, 2019, **150**, 1–10, 114305, (*d*) A. A. Gurinov, G. S. Denisov, A. O. Borissova, A. S. Goloveshkin, J. Greindl, H.-H. Limbach and I. G. Shenderovich, *J. Phys. Chem. A*, 2017, **121**, 8697–8705.
63 V. V. Mulloyarova, I. S. Giba, M. A. Kostin, G. S. Denisov, I. G. Shenderovich and P. M. Tolstoy, *Phys. Chem. Chem. Phys.*, 2018, **20**, 4901–4910.
64 R. M. Denton, J. An, B. Adeniran, A. J. Blake, W. Lewis and A. M. Poulton, *J. Org. Chem.*, 2011, **76**, 6749–6767.
65 H. C. E. McFarlane and W. McFarlane, Oxygen, in *Multinuclear NMR*, ed. J. Mason, Plenum Press, New York, 1987.
66 R. Curci, G. Fusco, O. Sciacovelli and L. Troisi, *J. Mol. Catal.*, 1985, **32**, 251–257.
67 J. J. Barieux and J. P. Schirmann, *Tetrahedron Lett.*, 1987, **28**, 6443–6446.
68 A. L. Baumstark, P. C. Vasquez and P. Balakrishnan, *Tetrahedron Lett.*, 1985, **26**, 2051–2054.
69 B. Plesničar, J. Cerkovnik, T. Tekavec and J. Koller, *Chem. – Eur. J.*, 2000, **6**, 809–819.
70 M. Căsný, D. Rehder, H. Schmidt, H. Vilter and V. Conte, *J. Inorg. Biochem.*, 2000, **80**, 157–160.
71 T. M. Alam, M. Celina, R. A. Assink, R. L. Clough, K. T. Gillen and D. R. Wheeler, *Macromolecules*, 2000, **33**, 1181–1190.
72 A. Wong, K. J. Pike, R. Jenkins, G. J. Clarkson, T. Anupõld, A. P. Howes, D. H. G. Crout, A. Samoson, R. Dupree and M. E. Smith, *J. Phys. Chem. A*, 2006, **110**, 1824–1835.
73 D. L. Bryce, K. Eichele and R. E. Wasylishen, *Inorg. Chem.*, 2003, **42**, 5085–5096.
74 H. Dahn, V. V. Toan and M.-N. Ung-Truong, *Magn. Reson. Chem.*, 1992, **30**, 1089–1096.
75 R. D. Sammons, P. A. Frey, K. Bruzik and M.-D. Tsai, *J. Am. Chem. Soc.*, 1983, **105**, 5455–5461.
76 H. Günzler and H.-U. Gremlich, *IR-Spektroskopie*, Wiley-VCH, 4th edn, 2003.
77 W. H. Fletcher and J. S. Rayside, *J. Raman Spectrosc.*, 1974, **2**, 3–14.
78 M. Hayyan, M. A. Hashim and I. M. AlNashef, *Chem. Rev.*, 2016, **116**, 3029–3085.
79 R. C. Taylor and P. C. Cross, *J. Chem. Phys.*, 1956, **24**, 41–44.
80 P. A. Giguére and T. K. K. Srinivasan, *J. Raman Spectrosc.*, 1974, **2**, 125–132.
81 H. H. Eysel and S. Thym, *Z. Anorg. Allg. Chem.*, 1975, **411**, 97–102.
82 V. Vacque, B. Sombret, J. P. Huvenne, P. Legrand and S. Suc, *Spectrochim. Acta, Part A*, 1997, **53**, 55–66.